Ridge-width dependence of the threshold of long wavelength (λ ≈14 μm) quantum cascade lasers with sloped and vertical sidewalls

Xue Huang,[1,*] Yenting Chiu,[1] William O. Charles,[1,2] and Claire Gmachl[1]

[1]*Department of Electrical Engineering, Princeton University, Princeton, New Jersey 08544, USA*
[2]*Current address: Photonic Devices, Inc., Raleigh, North Carolina 27606, USA*
[*]*xuehuang@princeton.edu*

Abstract: We investigate the ridge-width dependence of the threshold of Quantum Cascade lasers fabricated by wet and dry etching, respectively. The sloped sidewalls resulting from wet etching affect the threshold in two ways as the ridge gets narrower. First, the transverse modes are deeper in the substrate, hence reducing the optical confinement factor. Second, more important, a non-negligible field exists in the lossy SiO_2 insulation layer, as a result of transverse magnetic mode coupling to the surface plamon mode at the insulator/metal surface, which increases the waveguide loss. By contrast, dry etching is anisotropic and leads to waveguides with vertical sidewalls, which avoids the shift of the modes to the substrate layer and coupling to the surface plasmons, resulting in improved threshold compared with wet-etched lasers, e.g., for narrow ridge widths below 20 μm, the threshold of a 14 μm wide λ ≈14 μm laser by dry etching is ~60% lower than that of a wet-etched laser of the same width, at 80 K.

OCIS codes: (140.3070) Infrared and far-infrared lasers; (230.5590) Quantum-well, -wire and -dot devices.

References and links

1. M. Troccoli, X. Wang, and J. Fan, "Quantum cascade lasers: high-power emission and single-mode operation in the long-wave infrared (λ > 6 μm)," Opt. Eng. **49**(11), 111106 (2010).
2. N. Bandyopadhyay, Y. Bai, B. Gokden, A. Myzaferi, S. Tsao, S. Slivken, and M. Razeghi, "Watt level performance of quantum cascade lasers in room temperature continuous wave operation at λ ~ 3.76 μm," Appl. Phys. Lett. **97**(13), 131117 (2010).
3. S. Slivken, A. Evans, W. Zhang, and M. Razeghi, "High-power, continuous-operation intersubband laser for wavelengths greater than 10 μm," Appl. Phys. Lett. **90**(15), 151115 (2007).
4. K. Fujita, M. Yamanishi, T. Edamura, A. Sugiyama, and S. Furuta, "Extremely high T_0 values (– 450) of long wavelength (–5 μm), low-threshold-current-density quantum cascade lasers based on the indirect pump scheme," Appl. Phys. Lett. **97**(20), 201109 (2010).
5. X. Huang, W. O. Charles, and C. Gmachl, "Temperature-insensitive long-wavelength (λ ≈14 μm) Quantum Cascade lasers with low threshold," Opt. Express **19**(9), 8297–8302 (2011).
6. P. Fuchs, J. Semmel, J. Friedl, S. Höfling, J. Koeth, L. Worschech, and A. Forchel, "Distributed feedback quantum cascade lasers at 13.8 μm on indium phosphide," Appl. Phys. Lett. **98**(21), 211118 (2011).
7. S. Slivken, J. S. Yu, A. Evans, J. David, L. Doris, and M. Razeghi, "Ridge-width dependence on high-temperature continuous-wave quantum-cascade laser operation," IEEE Photon. Technol. Lett. **16**(3), 744–746 (2004).
8. W. Bewley, C. Canedy, C. S. Kim, M. Kim, J. R. Lindle, J. Abell, I. Vurgaftman, and J. Meyer, "Ridge-width dependence of midinfrared interband cascade laser characteristics," Opt. Eng. **49**(11), 111116 (2010).
9. R. P. Leavitt, J. L. Bradshaw, K. M. Lascola, G. P. Meissner, F. Micalizzi, F. J. Towner, and J. T. Pham, "High-performance quantum cascade lasers in the 7.3- to 7.8-μm wavelength band using strained active regions," Opt. Eng. **49**(11), 111109 (2010).
10. C. Gmachl, F. Capasso, A. Tredicucci, D. L. Sivco, A. L. Hutchinson, and A. Y. Cho, "Long wavelength (λ ≃ 13 μm) quantum cascade lasers," Electron. Lett. **34**(11), 1103–1104 (1998).
11. A. Tredicucci, C. Gmachl, F. Capasso, D. L. Sivco, A. L. Hutchinson, and A. Y. Cho, "Long wavelength superlattice quantum cascade lasers at λ ≃ 17 μm," Appl. Phys. Lett. **74**(5), 638–640 (1999).
12. R. Kitamura, L. Pilon, and M. Jonasz, "Optical constants of silica glass from extreme ultraviolet to far infrared at near room temperature," Appl. Opt. **46**(33), 8118–8133 (2007).
13. S. A. Maier, *Plasmonics: Fundamentals and Applications* (Springer, 2007).

#159075 - $15.00 USD Received 1 Dec 2011; revised 1 Jan 2012; accepted 9 Jan 2012; published 19 Jan 2012

14. F. Toor, D. L. Sivco, H. E. Liu, and C. F. Gmachl, "Effect of waveguide sidewall roughness on the threshold current density and slope efficiency of quantum cascade lasers," Appl. Phys. Lett. **93**(3), 031104 (2008).
15. Z. Liu, "Room-temperature, continuous-wave Quantum Cascade lasers in the first and second atmospheric windows," Ph.D. dissertation (Princeton University, 2008)

1. Introduction

Significant improvements on λ ~3.8 - 12.0 μm Quantum Cascade (QC) lasers have been achieved during the past few years [1–3]. In comparison, laser performance in the longer wavelength range, λ > 12.0 μm, has received less attention and is still under active, ongoing investigation [4–6]. Optimization of a QC laser includes optical gain, electron transport, mode confinement and optical loss, amongst other factors. Optical gain and electron transport are determined by the active core design alone. However, mode confinement and optical loss are mostly determined by the laser waveguide design. At the same time fabrication techniques, especially the etching method, also affect mode confinement and optical loss.

Two etching approaches are widely used in QC laser fabrication, wet etching by acid solutions, and dry etching by ion bombardment and vapor phase etchant. The advantages of wet etching include low cost, simple implementation, and smooth etching surface. However, wet etching, as most frequently applied to QC lasers, is isotropic and leads to a non-uniform ridge width, changing with the etch depth. For example, a wet-etched laser ridge with a width of 8 μm at the center of the active core is shown in Fig. 1(a), the active core of which has a 4.5 μm wide top and a 14.8 μm wide bottom. By contrast, dry etching provides vertical sidewalls and uniform ridge width as a result of anisotropic etching. Nevertheless it is a complex process where imbalance between physical etching and chemical etching, and bi-products from etching can all affect the etching profile and lead to sidewall roughness. In short, wet etching results in smooth surface and sloped sidewalls, while dry etching leads to vertical sidewalls, uniform ridge width, and increased roughness of the sidewalls.

For ridge waveguide lasers, the ridge width is also an important parameter related to threshold current and power consumption. A narrower width generally means better thermal dissipation, but also higher threshold current density. Published research demonstrated the ridge-width dependence of QC lasers in the shorter wavelength range, e.g., for a λ ≈6 μm laser by wet etching [7], and a λ ≈3.7 μm laser by dry etching [8], where a 12 μm wide laser in [7] and a 10 μm wide laser in [8] show the lowest threshold current densities in cw mode, respectively. A 2D simulation for QC lasers with λ~7.3- 7.8 μm showed that as the ridge width decreases, the increase in threshold current density of devices with vertical sidewalls (by dry etching) is lower than that of devices with sloped sidewalls (by wet etching), since the TM mode has a negligible tangential component at the vertical sidewall interfaces, and therefore the sidewall absorption in structures with vertical sidewalls is lower than in structures with sloping sidewalls [9].

For longer wavelengths, λ > 12 μm, the larger mode size makes it challenging to narrow the ridge width without deteriorating the laser performance, since the laser modes suffer from loss from the sidewall insulation layer and roughness, as well as a reduced mode confinement factor. Our motivation here is to optimize the geometry of waveguides for long wavelength QC lasers, and to reduce the ridge width without deteriorating the laser threshold, which is meaningful for cw mode operation and efficient thermal dissipation.

We investigate the threshold dependence on ridge width by both 2D mode simulation and threshold measurement, and show the difference in mode confinement and waveguide loss of lowest order transverse modes in wet-etched and dry-etched ridges. We find that the main challenges for narrowing wet-etched ridges include mode shift into the substrate and mode coupling to surface plasmon modes at the insulator/metal interface of sloped sidewalls. The former leads to decrease in confinement factor, while the latter results in high waveguide loss and is in fact the dominant factor for threshold increase as the ridge width decreases. By contrast, dry-etched ridges prevent mode shift by providing uniform lateral mode confinement unchanged with etch depth, and avoid mode coupling to surface plasmon modes due to the absence of transverse magnetic polarization for the vertical insulator and metal layers. As a

#159075 - $15.00 USD Received 1 Dec 2011; revised 1 Jan 2012; accepted 9 Jan 2012; published 19 Jan 2012

result, dry-etched QC lasers show lower threshold compared with wet-etched lasers, especially for narrow ridge width below 20 μm, e.g., the threshold of a 14 μm wide λ ≈14 μm QC laser by dry etching is ~60% lower than that by wet etching. Moreover, for dry-etched lasers, a sharp increase in threshold current density with narrowing ridge width is seen for ridge width below 14 μm, while for wet-etched lasers, the sharp increase in threshold current density appears already as the ridge width narrows below 20 μm. Therefore, dry etching is more preferable for long-wavelength QC lasers with narrow ridges.

2. Wet-etched λ ~14 μm QC lasers

The QC structure (structure A) used for wet etched laser fabrication is the same as the one reported earlier in [5]. Laser ridges were etched by an aged acid solution of HBr: HNO_3: H_2O = 1: 1: 10 after photolithography. The etching rate is about 1.2 μm/min, and the etching depth is 13.5 μm, with different average ridge widths of the active core from 14 to 35 μm. 3000 Å thick SiO_2 is then deposited by plasma-enhanced chemical vapor deposition (PECVD) for sidewall electrical insulation. Windows are opened for electric injection from the top of the ridges by reactive-ion etching (RIE) with O_2 and CF_4. The devices are thinned to ~200 μm after the top Ti/Au (200/3000 Å) contact is deposited by e-beam evaporation. Then a bottom Ge/Au (300/2000 Å) contact is deposited on the InP substrate. Finally the ridges are cleaved to Fabry–Pérot (FP) cavities and mounted epitaxial-side up to copper heat sinks.

Previously a low threshold current density of 2.0 kA/cm^2 was achieved from 2.8 mm long, λ ~14 μm lasers with HR-coated back facets at room temperature [5]. Here, since a large number of lasers are characterized for comparison, a shorter cavity length of 1.5 mm is chosen to obtain more lasers from the same area of processed sample, hence removing variations across the wafer. Nonetheless, the cavity length does not impact the generality of our research on the ridge-width dependence of the threshold which stems from the waveguide loss, since the cavity length only changes the mirror loss.

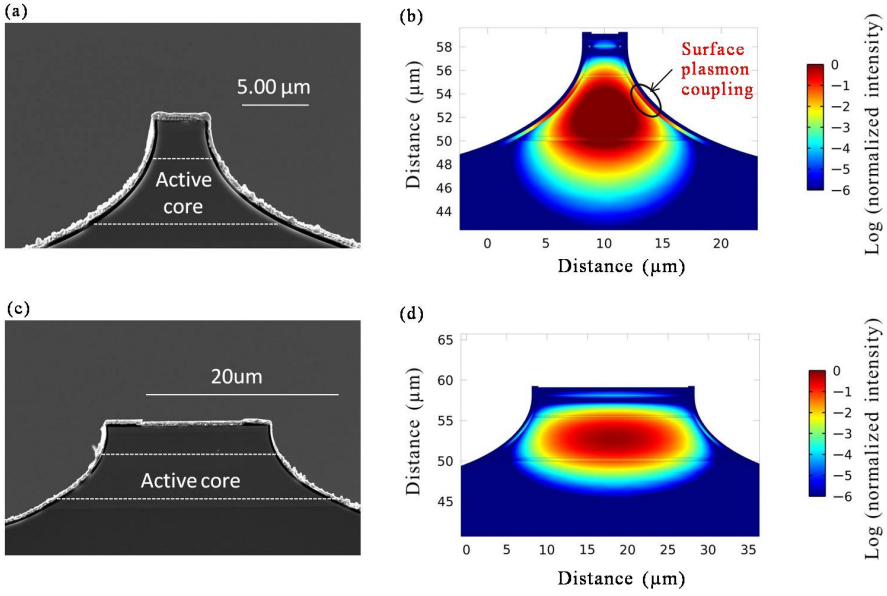

Fig. 1. (a) SEM picture of the cleaved laser facet of an 8 μm wide laser. (b) 2D simulation of the fundamental mode in an 8 μm wide QC laser. (c) SEM picture of the cleaved laser facet of a 24 μm wide laser. (d) 2D simulation of optical transverse mode in a 24 μm wide wet-etched QC laser

As a result of the isotropic property of wet etching, the etched ridges have sloped sidewalls, which plays an important role in optical mode confinement and insulation layer

#159075 - $15.00 USD Received 1 Dec 2011; revised 1 Jan 2012; accepted 9 Jan 2012; published 19 Jan 2012

absorption loss. It is worth noting that in fact the widely used SiO_2 insulation layer for long-wavelength ($\lambda \geq 13\mu m$) lasers ([5, 6, 10, 11]) is still lossy. The refractive index of SiO_2 is n = 1.82, and the extinction coefficient is $\kappa = 0.07$ for $\lambda \approx 14$ μm light [12]. The two-dimensional (2D) simulation (by the commercial software package COMSOL) of the lowest order transverse magnetic (TM) mode in wet-etched ridges from the $\lambda \sim 14\mu m$ QC structure under investigation is shown in Fig. 1. Compared to the 24 μm wide laser ridge, the mode in the 8 μm wide ridge is different in two ways. First, the mode is located further down in the lower $In_{0.53}Ga_{0.47}As$ waveguide layer and InP substrate, hence reducing the optical confinement factor Γ (= 83.5% for a 24 μm wide laser, and 72.4% for an 8 μm wide laser). Second, a non-negligible optical field exists in the SiO_2 insulation layer which covers the ridge sidewall, as a result of TM field coupling to the surface plasmons at the dielectric-metal interface. This leads to higher waveguide loss α_w (= 8.4 cm^{-1} for the 24 μm wide laser, and 26.9 cm^{-1} for the 8 μm wide laser). The additional loss caused by surface plasmon mode coupling at the insulator/metal interface on the sloped sidewalls is due to absorption in both the insulation layer and in the metal. However, the loss due to absorption in metals is estimated to be 3 orders of magnitude smaller than that in the insulation layer. Therefore, the loss due to absorption in the insulation layer is dominant. Compared with the 24 μm wide laser, the confinement factor of the 8 μm wide laser is decreased by 13.3%, and the waveguide loss is increased by 220%. Evidently, the increase in waveguide loss is more significant than the decrease in the confinement factor, and is the dominant factor for threshold increase as the ridge width decreases. It is worth noting that surface plasmon polaritons only exist for TM polarization (with the electric field perpendicular to the interfaces) at insulator/metal interfaces [13]. In the active core, polarization selection rules for intersubband transitions require a TM mode with the electric field perpendicular to the epilayers, hence generating an electric component perpendicular to the insulator and metal layers covering the sloped sidewall, which is coupled to the surface plasmon mode (TM mode with respect to the side walls) at the insulator/metal interface and causes the extra loss.

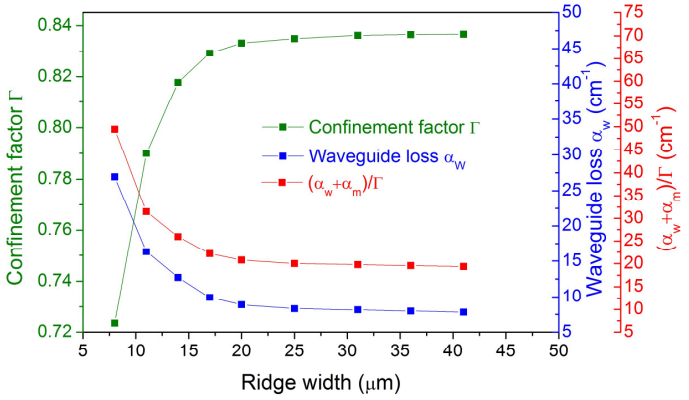

Fig. 2. 2D simulation results of confinement factor, waveguide loss, and loss-confinement ratio dependence on ridge width. The FP cavity length is assumed to be 1.5 mm for mirror loss α_m calculation.

Since the threshold current density is related to both the confinement factor Γ and the waveguide loss α_w by

$$J_{th} = (\alpha_W + \alpha_m)/(g \cdot \Gamma) \propto (\alpha_W + \alpha_m)/\Gamma \qquad (2)$$

where α_m is the mirror loss, and g is the gain coefficient, the threshold current density will be changed accordingly as the ridge width changes. In Fig. 2, 2D simulation results of α_w, Γ, and $(\alpha_w + \alpha_m)/\Gamma$ are plotted versus average ridge width for 1.5 mm long FP lasers, which predicts significant increase in threshold current density as the ridge width decreases below 20 μm.

#159075 - $15.00 USD Received 1 Dec 2011; revised 1 Jan 2012; accepted 9 Jan 2012; published 19 Jan 2012

For example, a 24% increase in threshold is predicted by simulation, when the ridge width is decreased from 20 μm to 14 μm.

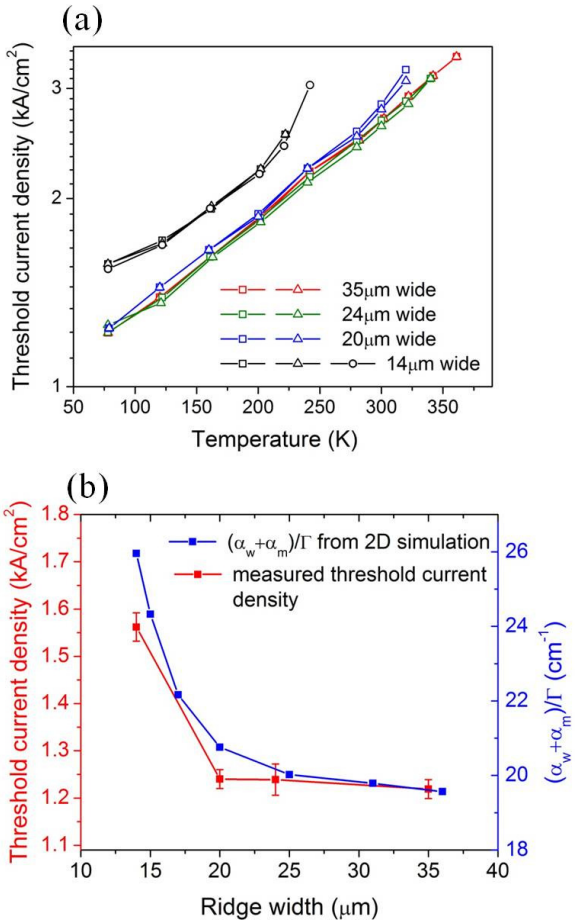

Fig. 3. (a) Threshold current density of 1.5 mm long, wet-etched QC lasers with different ridge widths from 14μm to 35μm in pulsed mode, from 80 K to 350 K. The pulse width is 100 ns, and the repetition rate is 4 kHz. (b) Simulated loss-confinement factor ratio and measured threshold current density at 80 K, of 1.5 mm long, wet-etched QC lasers with different ridge widths from 14μm to 35μm. The measured threshold current density versus the ridge width is plotted with error bars obtained from the threshold variations for lasers of the same ridge width.

Temperature-dependent threshold measurement results of 1.5 mm long, as-cleaved lasers with different ridge widths from 14 μm to 35 μm in pulsed mode are shown in Fig. 3(a). The threshold current density at 80 K and simulated $(\alpha_w + \alpha_m)/\Gamma$ versus ridge width are plotted in Fig. 3(b). Please note that the waveguide loss calculated from the 2D simulations is expected to best predict the waveguide loss of devices operating at cryogenic temperature. For QC lasers operating at high temperatures, the total waveguide loss includes contributions from thermal backfilling and thermal leakage, which are not included in the 2D mode simulations. From the characterization, for laser ridges above 20 μm wide, the threshold current density is insensitive to ridge width. Compared to the 35 μm wide laser, the threshold of the 20 μm wide laser only increases by less than 5%. However, as the ridge width decreases from 20 μm to 14 μm, the threshold current density is increased by about 26%, close to the simulated increase 24%. Due to this sharp increase in threshold, the 14 μm wide QC lasers only operate up to 240 K, as shown in Fig. 3(a).

#159075 - $15.00 USD Received 1 Dec 2011; revised 1 Jan 2012; accepted 9 Jan 2012; published 19 Jan 2012

From the discussion above, the sloped sidewalls result in high threshold current densities for wet-etched QC lasers with narrow ridge widths (below 20 µm for lasers under investigation here). However, as the most frequently employed etching technique in QC laser fabrication, wet etching features some desirable advantages including low cost, simple implementation, and smooth etch surfaces. It would be meaningful to minimize the influences of sloped sidewalls on the threshold current density in wet-etched lasers with narrow ridges. This can be improved by employing a thicker $In_{0.53}Ga_{0.47}As$ upper waveguide layer (doped n~5×10^{16} cm^{-3}), with other layers unchanged. By increasing it from the original thickness of 0.2µm to 1.5 µm in 2D mode simulation for an 8 µm wide laser, the confinement factor is increased by 7%, since the laser mode is located higher in the active core. At the same time, the TM component with respect to the sidewall is decreased, since the sidewall is less sloped in the upper part than the lower part of the active core. As a result, the waveguide loss is decreased by 16% for the 8 µm wide laser, owing to weaker TM mode coupling to surface plasmons at the insulator/metal interface.

3. Dry-etched λ ~14 µm QC lasers

A similar sample (structure B) emitting at 14 µm is used for dry-etching fabrication. QC lasers under test are fabricated with inductively coupled plasma reactive-ion etching (ICP-RIE). A SiN_x hard mask is transferred from photolithography by RIE based on O_2 and CF_4 gases. Then 11 µm deep ridges are etched by $Cl_2/SiCl_4/Ar$ ICP-RIE. After removing the SiN_x hard mask, the deposition of the SiO_2 insulation layer, window opening, and contact evaporation steps are the same as described above for the wet-etched ridges.

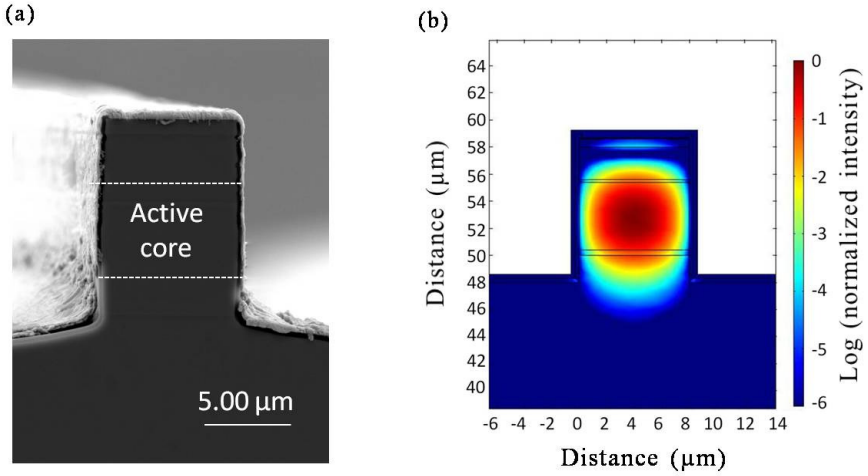

Fig. 4. (a) SEM picture of the cleaved laser facet of an 8 µm wide dry-etched laser. (b) 2D simulation of the fundamental mode in an 8 µm wide dry-etched QC laser.

Due to the vertical sidewalls from the dry etching, the laser ridges provide uniform confinement for optical modes independent of etch depth. Different from wet-etched lasers shown in Fig. 1, here no surface plasmon mode coupling is seen in the insulation layer of the 8 µm wide dry-etched laser in Fig. 4. The TM mode in the active core corresponds to a transverse electric (TE) mode with respect to the sidewalls, with its polarization totally parallel to the interface, in the insulation layer and metal layers. However, no surface plasmon modes exist for TE polarization at insulator/metal interfaces [13]. Therefore, the dry-etched ridges width vertical side walls avoid mode coupling to surface plasmon modes at the insulator/metal interface.

In Fig. 5, simulation results of α_w, Γ, and $(\alpha_w + \alpha_m)/\Gamma$ are plotted versus ridge width for 1.5 mm long dry-etched FP lasers with as-cleaved facets. For comparison, simulated $(\alpha_w + \alpha_m)/\Gamma$ of wet etched ridges, which was shown earlier in Fig. 2, is also plotted in Fig. 5.

#159075 - $15.00 USD Received 1 Dec 2011; revised 1 Jan 2012; accepted 9 Jan 2012; published 19 Jan 2012

Evidently, the absence of surface plasmon modes at the semiconductor/metal interface of dry-etched lasers leads to lower $(\alpha_w + \alpha_m)/\Gamma$, thus lower threshold compared with wet-etched lasers, especially for ridge widths below 20μm.

In [9], $(\alpha_w + \alpha_m)/\Gamma$ is increased by 8% as the ridge width decreases from 15 μm to 7 μm from 2D simulation for the λ ~7.3- 7.8 μm QC laser with vertical sidewalls. By comparison, here seen from Fig. 5, $(\alpha_w + \alpha_m)/\Gamma$ is increased by 15% as the ridge width decreases from 15 μm to 7 μm for the λ ~14 μm QC laser with dry-etched vertical sidewalls. Therefore, the increase in $(\alpha_w + \alpha_m)/\Gamma$ of the λ ~14 μm dry-etched laser is larger than that of the λ ~7.3- 7.8 μm dry-etched laser as the ridge width decreases from 15 μm to 7 μm, since the longer-wavelength mode has a larger mode size, hence it is more sensitive to ridge width narrowing.

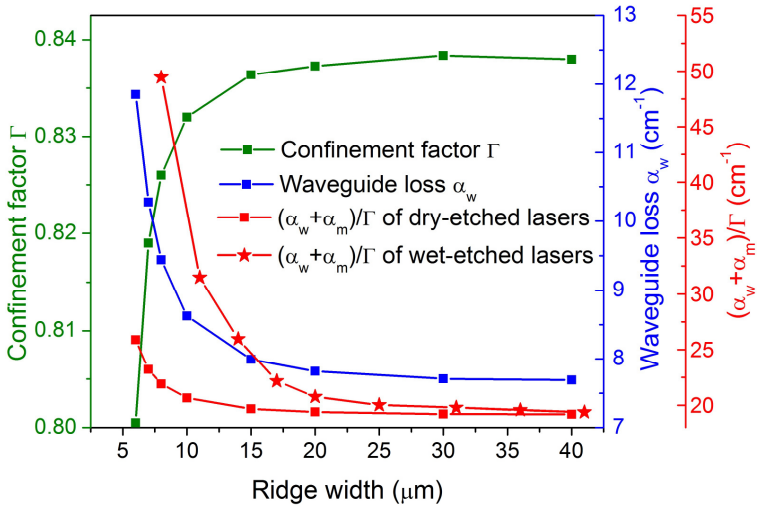

Fig. 5. 2D simulation results of confinement factor and waveguide loss from dry-etched lasers, and loss-confinement ratio of both wet-etched and dry-etched lasers. The FP cavity length is assumed to be 1.5 mm for mirror loss α_M calculation.

Temperature-dependent threshold current measurements of 1.5 mm long, as-cleaved λ ~14 μm QC lasers fabricated by dry etching with different ridge widths from 8 μm to 26 μm are shown in Fig. 6(a). Also shown in the inset is the threshold current density versus ridge width of dry-etched QC lasers, as well as that of wet-etched QC lasers from the same wafer, both at 80 K.

The dry-etched lasers show lower threshold current density than the wet-etched lasers. For wide ridge width above 20 μm, the former is 25% lower than latter. For narrower ridge width below 20 μm, the waveguide loss of wet-etched lasers is significantly increased, as shown in Fig. 2, owing to mode coupling to surface plasmons at the sidewall insulator/metal interface. By contrast, the vertical sidewalls of dry-etched lasers avoid surface plasmon mode coupling at the sidewall insulator/metal interface. As a result, the threshold current density of dry-etched lasers is significantly lower than wet-etched ones. For 14 μm wide lasers under test here, the former is 60% lower than the latter, seen from the inset of Fig. 6(a).

A clear increase in threshold happens when the ridge width narrows to below 14 μm for dry-etched lasers. Both the measurement threshold current density and the simulation results are shown in Fig. 6(b). The threshold increases faster with decreasing ridge width than predicted by simulation, e.g., as the ridge width decreases from 14 μm to 9 μm, the threshold is predicted to increase by 8.1%, while from the experimental results it increases by 44%. This difference is attributed to non-negligible sidewall roughness generated by ICP- RIE, which is not included in the simulation [14].

#159075 - $15.00 USD Received 1 Dec 2011; revised 1 Jan 2012; accepted 9 Jan 2012; published 19 Jan 2012

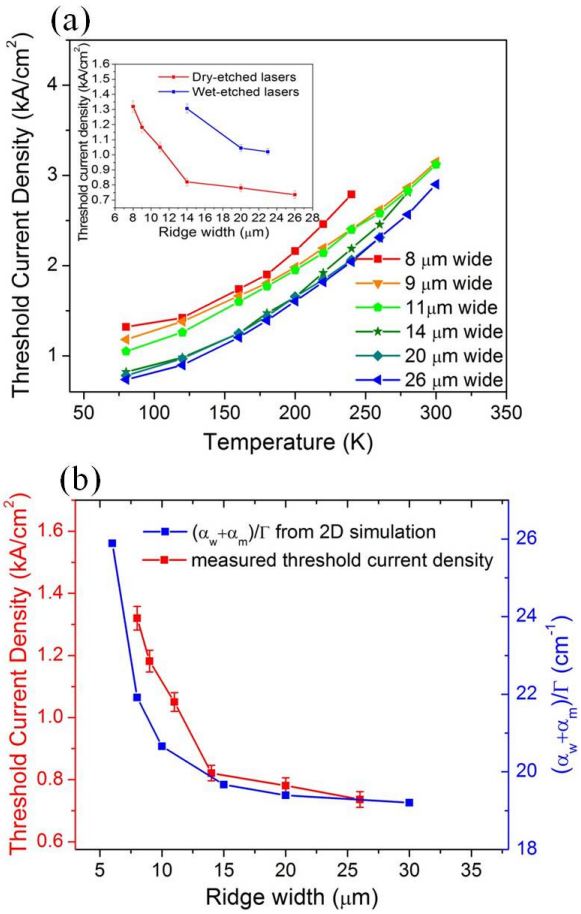

Fig. 6. (a) Threshold current density of 1.5 mm long, dry-etched QC lasers with different ridge widths from 8 μm to 26 μm, in pulsed mode. The pulse width is 100 ns, and the repetition rate is 4 kHz. The inset shows the threshold current density of dry-etched and wet-etched lasers with different ridge widths at 80 K. (b) Simulated loss-confinement factor ratio and measured threshold current density, of 1.5 mm long, dry-etched QC lasers with different ridge widths.

From Fig. 6(a), the dry-etched QC lasers operate only up to 300 K, with a threshold current density around 3.0 kA/cm^2 at 300 K. This relatively high threshold is due to thermal backfilling at non-cryogenic temperature. The QC structure (structure B) used for dry-etched devices shown in Fig. 6 (as well as the wet-etched devices shown in Fig. 6(a)) is different from the structure (structure A) used in [5]. More specifically, a significant change is that compared to structure A, the injector thickness of each stage in structure B is reduced by 6.9 nm, and the energy difference between the lower laser state and the upper laser state in the next stage is reduced by ~20 meV, leading to higher thermal backfilling at non-cryogenic temperatures. The deterioration in high temperature performance of structure B is also seen from a lower characteristics temperature T_0 fit by the empirical exponential function $J_{th}(T) = J_0*exp(T/T_0)$. For example, the characteristics temperature T_0 obtained for the 14 μm wide dry-etched laser (from structure B) shown in Fig. 6(a) is 160 K, much lower than T_0 ~300 K obtained in [5] with structure A. As a result, the 14 μm wide dry-etched laser from structure B here only operates up to 280 K with a high threshold current density of 2.8 kA/cm^2, while the laser from structure A in [5] operates up to 350 K with a threshold of 2.95 kA/cm^2 at 350 K and 2.5 kA/cm^2 at 300 K. Therefore, the high threshold obtained here at room temperature is due to thermal backfilling in the active core design of structure B. But since our goal here is to compare ridge-width dependence of the threshold of wet-etched and dry-etched lasers,

#159075 - $15.00 USD Received 1 Dec 2011; revised 1 Jan 2012; accepted 9 Jan 2012; published 19 Jan 2012

without loss of generality we have the conclusion that the dry-etched lasers with vertical sidewalls are more preferable for narrow ridges (below 20 μm).

The dry-etched lasers failed to operate in cw mode due to the high threshold, as well as inefficient heat dissipation with the $In_{0.52}Al_{0.48}As$ cladding layers and the thin Au contact (~300 nm). The goal for the next step is to achieve cw operation with λ ~14 μm dry-etched QC lasers. For initial comparison of the thermal dissipation for dry-etched and wet-etched lasers, the pulsed temperature-dependent threshold of 14 μm wide dry-etched and wet-etched lasers in Fig. 6(a) are used for thermal modeling by self-consistent iteration with COMSOL to calculate the threshold in cw mode at 80 K [15]. By simulation, the cw threshold current density of the 14 μm wide dry-etched laser is 1.0 kA/cm^2 with a core temperature of 122 K in the active core, while the cw threshold of the 14 μm wide wet-etched laser is 1.9 kA/cm^2 with a core temperature of 165 K. Therefore, from the estimation based on thermal modeling, the threshold of the 14 μm wide wet-etched laser is 90% higher than that of the 14 μm wide dry-etched laser at 80 K.

4. Conclusion

In summary, we have studied the ridge-width dependence of the threshold current density of long wavelength (λ ~14 μm) QC lasers, with ridges defined by wet etching and dry etching, respectively. The dry-etched lasers show improved threshold compared with wet-etched lasers from both 2D mode simulation and experimental results.

For lasers with narrow ridges (below 20 μm for lasers under investigation here), the sloped sidewalls fabricated by wet etching significantly affect the threshold in two ways. First, as the wet-etched ridge gets narrower, the transverse mode are located further down in the substrate, which decreases the confinement factor. Second, more important, a non-negligible field exists in the lossy SiO_2 insulation layer, as a result of TM field coupling to the surface plasmon mode at the insulator/metal interface, which increases the waveguide loss. For example, compared to a 24 μm wide laser, the confinement factor of an 8 μm wide laser is decreased by 13.3%, and the waveguide loss is increased by 220% from 2D mode simulation. Evidently, the high waveguide loss caused by mode coupling to surface plasmons is the dominant factor for threshold increase as the wet-etched ridge becomes narrower. By contrast, dry-etched ridges can prevent mode shift to the substrate layer as a result of uniform lateral mode confinement unchanged with etch depth. More important, it also avoids mode coupling to surface plasmon polaritons at the insulator/metal interface, since no TM polarization exists with respect to the vertical insulator and metal layers. As a result, for narrow ridge width (below 20 μm for devices tested here), the threshold current density of a dry-etched laser is significantly lower than that of a wet-etched laser with the same ridge width, e.g., the threshold current density of a 14 μm wide dry-etched laser by is 60% lower than that of a 14 μm wide wet-etched. Moreover, for dry-etched lasers, a sharp increase in threshold current density with narrowing ridge width is seen for ridge width below 14 μm, while for wet-etched lasers, the sharp increase in threshold current density appears already as the ridge width narrows below 20 μm. Therefore, dry etching is more preferable for long-wavelength QC lasers with narrow ridges.

Acknowledgments

This work is supported in part by MIRTHE (NSF-ERC).

#159075 - $15.00 USD Received 1 Dec 2011; revised 1 Jan 2012; accepted 9 Jan 2012; published 19 Jan 2012